16th ICAAR LISBOA 2020-2022

16th International Conference on
Alkali-Aggregate Reaction in Concrete
Lisboa | LNEC | Portugal | 31 May - 2 June 2022

http://icaar2020-2022.lnec.pt

Applying the Damage Rating Index for the spatial damage assessment in concrete specimens affected by alkali-silica reaction

Mathieu Champagne[(1)], Jan Lindgård[(2)], Benoit Fournier[(3)], Josée Duchesne[(4)]

(1) *Laval University, Québec City, Canada, mathieu.champagne.8@ulaval.ca*

(2) SINTEF Building and Infrastructure, Trondheim, Norway, jan.lindgard@sintef.no

(3) *Laval University, Québec City, Canada, benoit.fournier@ggl.ulaval.ca*

(4) *Laval University, Québec City, Canada, josee.duchesne@ggl.ulaval.ca*

Abstract

With the raising popularity of the Damage Rating Index (DRI) method as a concrete damage assessment tool, the potential of this method to apply spatial damage assessment, i.e. identifying damage variations within the same specimen, was investigated. This was conducted on a series of 30 concrete prisms after being tested for alkali-silica reactivity with various concrete performance test procedures. The assessed prisms were manufactured with different aggregates and binders as well as being exposed to four different laboratory testing conditions. Two DRI spatial damage assessment tools were developed, i.e. the analysis of "grouped lines" and the "damage profile". The former consists in separating the specimen in grouped lines of equal distance (laterally) from the prism's surface and the latter consists in separating the prism in four zones of equal area from the top to the bottom of the prism.

The results indicate that the DRI method is "sensitive" enough for damage spatial assessment if local damage variations are present within a large enough area, i.e. ± 50 cm^2. Overall, the damage assessments showed that the internal damage generation is strongly dependent on the type of binder and on the exposure conditions. Moreover, alkali leaching from the prisms strongly impact damage development in the prisms (from top to bottom and from the interior to the edge). Furthermore, the paper discusses the "local race" between the reduction of alkalis due to leaching (reduces ASR) and the increase of damage enhanced by increased access to water.

Keywords: *alkali-silica reaction (ASR); concrete petrography; damage rating index (DRI); performance testing*

1. INTRODUCTION

Different concrete damage assessment tools were developed in the past to help engineers in the management of concrete structures affected by internal swelling reactions, such as alkali-silica reaction (ASR). One of them being the *Damage Rating Index* (DRI) method, which has increasingly been used over the last two decades either in research projects [1–9] or engineering practice [10–17], especially in North America. The DRI method is a petrographic damage assessment tool developed by P.E. Grattan-Bellew from the National Research Council of Canada [18]. It is performed with the use of a stereomicroscope (about 15x magnification) where damage features generally associated with ASR are counted by an operator through a 1 to 1.5 cm² grid drawn on the surface of a polished section. The number of counts corresponding to each selected petrographic feature is multiplied by weighting factors, whose purpose is to balance their relative importance towards the distress mechanism of interest, for instance ASR [3]. Each square is thereby summed up to obtain a numeric value, the *DRI number*, which is normalized to a 100 cm² area for ease of comparison.

Even if the DRI can reliably assess damage in concrete affected by ASR [1, 19], applying this tool for spatial damage assessment, i.e. identifying damage variations within the same specimen, is still largely unexplored. This potentially new way of using the DRI method, i.e. by providing more than just a number, could promote even more its use in research or engineering practice. Since such application highly depends on the "sensitivity" of the method, a same operator repeatability study conducted by the main author if this paper indicated that the uncertainty related to the operator should fall between the margin of error (*ME*) provided in the following [20]:

$$ME\ (\%) = \left(\frac{z_{1-\alpha/2}\sqrt{(0.4944 \cdot \overline{DRI} + 105.53)^2/n}}{\overline{DRI}} \right) \cdot 100 \quad (1)$$

where $z_{1-\alpha/2}$ is the value associated to the desired level of confidence (Table 1.1), n is the number of analysed cm^2 and $\overline{DRI}$ the DRI number of the analysed area. A very good coefficient of determination (≈ 0.99) was obtained in a replicate study of eight specimens into which the "punctual" standard deviation was estimated with a degree of freedom equal to 194 [20]. Therefore, Equation (1) was used in this study to reliably compare DRI numbers obtained within the same specimen with respect to the uncertainty related to the operator performing the test.

Table 1.1: Some (two-tails) $z_{1-\alpha/2}$ values depending on the confidence level (according to the Standard Normal Distribution), adapted from the Student *t*-distribution in Ramsey and Schafer [21].

Confidence level (%)	50	60	70	80	90	95	98	99
$z_{1-\alpha/2}$ values	0.674	0.842	1.036	1.282	1.645	1.960	2.326	2.576

2. SCOPE OF WORK AND OBJECTIVES

By having insights on the DRI's sensitivity applying the method for spatial damage assessment is potentially possible with any operator who assessed his/her own repeatability. As indicated in Equation (1), the capability of the latter ultimately depends on the size of the compared areas and the difference between their respective DRI numbers. Therefore, the objective of this study was to use Equation (1) to assess the capability of the DRI as a spatial damage assessment tool on a series of concrete prisms showing internal damage variations/patterns. The assessed prisms were indeed exposed to various accelerated test conditions and were manufactured from a wide range of mix design (binder types and reactive aggregates).

3. METHODOLOGY

3.1 Materials

The series of concrete prisms analysed in this study were cast and tested through the Norwegian COIN program (2007-2014; https://www.sintef.no/en/projects/coin/coinp/). The COIN experimental program was conducted in coordination with the activities of RILEM TC 219-ACS and TC 258-AAA, which focused mainly on improving current ASR test methods and develop a performance-based testing concept for the prevention of deleterious ASR [22, 23]. The test prisms were manufactured from different concrete mixtures (aggregates and binders) and were subjected to different laboratory testing conditions [22, 24, 25]. The prisms were all of the same size (70 x 70 x 280 mm). The water-to-binder ratio (w/b) was kept constant at 0.45 and the nominal cement content was 400 kg/m^3 in all mixtures, except a few rare cases where a nominal cement content of 440 kg/m^3 was used. To achieve an appropriate consistency, a small quantity of a low-alkali superplasticiser was added to some of the concrete mixtures. No air entraining agent was used. However, to avoid any influence on the ASR expansion of varying (entrapped) air content in the different test series, a small quantity of a de-foaming agent was added to the concrete mix when the air content was higher than 3.0%. The concrete samples were consolidated manually by rodding.

The prisms were either stored at 38°C in a temperature-controlled room in a plastic container with a lining of absorbent material in contact with the bottom water or at 60°C on grids above water in a metal container placed inside a "reactor" with 100 % relative humidity (RH), depending on the testing method used. The same edge of the prism was always oriented towards the top of the container, instead of changing the prism's orientation after each reading (like prescribed in most test methods). Furthermore, some prisms were wrapped with a cotton cloth moistened with an alkaline solution (pH 14.2) and then inserted in a polyethylene lay-flat tubing (prism ends not covered with cloth), as described in Table 3.1. As the unwrapped prisms, these wrapped prisms were stored on grids above water (100 % RH). In the case of the alkali wrapped prisms, 5 mL of water was poured on the upper end face of the prism (top edge) after each length-change reading.

Four out of the five coarse aggregates (i.e. fraction > 4 mm) used by Lindgård et al. [22, 24, 25] were selected for this study: “Spratt”, “Ottersbo”, “Upper Rhine” and “N3”. The “Spratt” is a crushed silicified limestone from Ontario (Canada) and has been used as a reference reactive aggregate in several studies around the world [26]. The “Ottersbo” is a crushed cataclasite from Norway and is used as a reference reactive aggregate in Norway [27]. The “Upper Rhine” is a German river gravel from the Upper Rhine region and contains impure limestone, marl, sandstone and a small proportion of cataclastic rocks. This gravel is used as a “reference” reactive aggregate in some German ASR tests [28]. According to Lindgård et al. [22], the reactive material in the above aggregates consists in crypto- to microcrystalline quartz. The “N3” is a natural and partly crushed gneiss/granite from Årdal (Norway) classified as non-reactive according to the Norwegian ASR regulations (tested by petrographic analysis). For all concrete mixtures, the fine fraction was a reference non-reactive and partly crushed sand from Årdal (Norway: the fine fraction of the “N3” aggregate).

After completion of the expansion testing, those prisms were wrapped in plastic sheets and stored until they were sent to Laval University to evaluate the extent of cracking and the potential damage variations inside the prisms using the DRI. The information regarding each prism analysed in this study is given in Table 3.2. The number of the test series represents the mix design used (e.g. 2U), while U means no air entrainment. The notation following the number represents the concrete prism test (CPT) method used (e.g. ASTM), which is described in Table 3.1. Further details regarding the COIN experimental program is provided in Lindgård et al. [22].

3.2 Methods

3.2.1 Specimen preparation

Upon their reception at Laval University, the concrete prisms were cut lengthwise and polished in wet conditions using a portable stone grinder with a range of diamond-impregnated resin polishing pads (no. 50 (coarse), 100, 400, 800, to 1500 to 3000 (very fine)). A grid was then drawn on the sections with squares of 1 cm by 1 cm in size. The specimen tag was hidden with a duct tape and a temporary name (unknown to the operator) was given to specimens to avoid any bias during DRI determination.

3.2.2 Damage Rating Index

The DRI method (see section 1) was performed over the whole area (196 cm^2) of all concrete specimens by an operator that had previously acquired experience on a wide variety of reactive rock types and mix designs (i.e. including supplementary cementitious materials (SCM) bearing concretes). As discussed in Champagne [20], the operator’s experience level was considered high enough to provide reliable and consistent results that follows the repeatability mentioned in Equation (1). The specimens were examined under a stereomicroscope with a magnification of 15x and petrographic features generally associated with ASR were counted within each square (cm^2). The number of counts corresponding to each type of petrographic features was multiplied by the weighting factors recommended by Villeneuve et al. [29] and the final value, referred as *DRI number*, was normalized to a 100 cm^2 area. Table 3.3 shows the damage features and their weighting factors used in the determination of the *DRI* number. These were selected because they are considered to induce lower single and multiple-operator variability. Moreover, the DRI numbers obtained with these weighing factors can reliably assess damage of concrete due to ASR in terms of expansion [19] and loss in mechanical properties [30]. The cracks were counted in the coarse aggregate and sand particles larger than 1 mm in diameter to consider also the reactivity of the sand (if any), as recommended by Sanchez et al. [31].

Table 3.1: Overall view of the concrete prism testing laboratory conditions applied by Lindgård et al. [22, 24, 25].

Based upon method	Notation (Table 3.2)	Pre-treatment[1]	Reference reading	Prism size (mm)	Storage conditions		Reading
					Temp. (°C)[2]	Humidity[3,4,5]	
Former RILEM AAR-3 [32]	**3.12**	Prism submerged in deionised water for 0.5 h after de-moulding.	24 h. after high temperature storage.	70 x 70 x 280	38 ± 2	Each prism wrapped[6] in a cotton cloth moistened with ~ 70-75 g of an alkaline solution (Na/K-ratio ≈ 1/3) of pH 14.2. Prisms inserted in a polyethylene lay-flat tubing (prism ends not covered) and then sealed inside a polyethylene bag.	Without pre-cooling[7].
Former RILEM AAR-4 Alternative [32]	**4.12**	Prism submerged in deionised water for 0.5 h after de-moulding.	24 h. after high temperature storage.	70 x 70 x 280	60 ± 2	Each prism wrapped[6] in a cotton cloth moistened with ~ 70-75 g of an alkaline solution (Na/K-ratio ≈ 1/3) of pH 14.2. Prisms inserted in a polyethylene lay-flat tubing (prism ends not covered) and then sealed inside a polyethylene bag.	Without pre-cooling[7].
RILEM AAR-4.1 [33]	**4.2**	Prism submerged in deionised water for 0.5 h after de-moulding	24 h. after high temperature storage.	70 x 70 x 280	60 ± 2	Unwrapped prisms (3) stored in a metal container (no lining), Several small containers stored inside a larger cabinet ("reactor") on grids over water.	Without pre-cooling[7].
ASTM C1293 [34]	**ASTM**	No submersion after de-moulding.	Directly after de-moulding.	70 x 70 x 280	38 ± 2	Unwrapped prisms (3) stored in a plastic container, inside wall of the container lined with a (damp) cloth with lower part immersed in deionised water in the bottom.	Pre-cooled prior to reading.

1. All prisms stored at ~ 20 °C under a plastic sheet for the first 24 h before de-moulding. Any subsequent pre-treatment prior to testing conditions is described below.
2. Except for the RILEM AAR 4.1 CPT ("reactor"), the containers were stored in a hot room or an oven.
3. In all CPTs, the prisms were stored vertically on grids above water, without being in direct contact with the water. A humid environment close to 100% RH is aimed.
4. The same end of the prism was always oriented towards the top, instead of changing the prism's orientation after each reading.
5. For all test methods the prisms (unwrapped and wrapped) were stored on grids above water inside their storage containers.
6. Each wrapped prism stored inside a separate polyethylene bag, 5 mL of deionised water poured over the upper end face before sealing the bag and after each reading. Sealed bag stored in a separate plastic container (with lining in contact with the bottom water).
7. According to the procedure described in Lindgård et al. [24].

Table 3.2: Overall mix design, laboratory testing conditions and expansion attained by the prisms analyzed in this study.

Mix no. and test method (Table 3.1)	Coarse Aggregate	Total Alkali content (kg/m³, Na_2O eq)[1]	Binder content (kg/m³)	Supplementary Cementitious material (SCM)[2]	Exposure time (weeks)	Submerged before reference reading[3]		Pre-cooled before reading		Alkali wrapping[4]		Exposure temperature (°C)		Expansion level (%)
						Yes	No	Yes	No	Yes	No	38	60	
1U-4.12	Spratt	1.5	400		52	√			√	√			√	0.022
2U-4.2		2.0			67	√			√		√		√	0.026
14U-4.12		4.0		Slag	95	√			√	√			√	0.028
10U-4.12		6.5		Fly ash	65	√			√	√			√	0.035
14U-4.2		4.0		Slag	95	√			√		√		√	0.039
2U-4.12		2.0			52	√			√	√			√	0.041
14U-ASTM		4.0		Slag	133		√	√			√	√		0.041
10U-3.12		6.5		Fly ash	126	√			√	√		√		0.075
3U-ASTM		2.9			131		√	√			√	√		0.216
2U-3.12		2.0			120	√			√	√		√		0.221
1U-3.12		1.5			120	√			√	√		√		0.234
3U-3.12		2.9			121	√			√	√		√		0.244
7U-ASTM	Ottersbo	5.0		Fly ash	119		√	√			√	√		0.025
7U-4.2		5.0		Fly ash	65	√			√		√		√	0.026
4U-4.2		2.0			65	√			√		√		√	0.032
13U-4.2		4.0		Slag	95	√			√		√		√	0.039
8U-4.2		6.5		Fly ash	65	√			√		√		√	0.053
8U-ASTM		6.5		Fly ash	121		√	√			√	√		0.055
13U-ASTM		4.0		Slag	134		√	√			√	√		0.055
21U-ASTM		9.0		Fly ash	112		√	√			√	√		0.088
4U-4.12		2.0			65	√			√	√			√	0.183
6U-4.2		3.7			66	√			√		√		√	0.230
6U-ASTM		3.7			52		√	√			√	√		0.254
17U-3.12	Upper Rhine	6.5		Fly ash	128	√			√	√		√		0.038
17U-4.2		6.5		Fly ash	103	√			√		√		√	0.054
15U-3.12		5.5			133	√			√	√		√		0.236
15U-ASTM		5.5			133		√	√			√	√		0.240
11U-ASTM	N3	5.5	440		117		√	√			√	√		0.100
11U-3.12		5.5			111	√			√	√		√		0.113
11U-4.2		5.5			151	√			√		√		√	0.314

1. Including all alkalis in the fly ash and the slag (if any).
2. SCM concretes contains 21.6 weight-% of class F fly ash or 34 weight-% of slag (ggbfs).
3. Concrete specimens were submerged for 0.5 h before being exposed to elevated temperature.
4. Some concrete specimens were wrapped with a cloth containing an alkaline solution (pH of 14.2), further details in Table 3.1.

Table 3.3: Petrographic features and weighing factors used in the determination of the *DRI number* [29].

Petrographic features		Acronyms	Weighing factor
Crack in the aggregate particles (> 1 mm)	*Closed (without reaction products)*	**CCA**	**0.25**
	Opened or in a fine network (without reaction products)	**OCA**	**2**
	Opened or in a fine network (with reaction products)	**CA + RP**	
Crack in the cement paste	*Without reaction products*	**CCP**	**3**
	With reaction products	**CCP + RP**	
Debonded aggregate (> 1 mm)		**Debon**	
Reacted aggregate particle (> 1 mm)		**RAP**	**2**

3.2.3 Spatial damage assessment

A new data processing tool for the DRI method was developed in this study to help understand how damage varies within a concrete specimen. While performing the DRI, the data are incorporated in a macro-programmed excel sheet that provides the DRI values of every square analysed. These "local" DRI values are determined by calculating the sum of the counted petrographic features multiplied by their respective weighting factor (Table 3.3), which is then rounded to the first decimal point. The interesting feature of this macro-programmed excel sheet is the possibility to evaluate/compare the DRI number of a selected number of squares from specific areas of interest within the same specimen.

In this study, one interest was to determine whether damage in the sides (i.e. moving along the cross-section) was different than that in the core of the specimen. For this purpose, the polished section was separated in three groups of two so-called *lines*, which were located at the same distance from the prism side surface, as shown in Figure 3.1. The single *line* in the middle of the prism was not considered due to the lower number of *squares* available for DRI determination. This spatial damage assessment tool is referred as the ***grouped lines approach***. Another interest was to investigate if a damage gradient was present from the top to the bottom edges of the prism due to alkali leaching, as it was always oriented in the same direction for the whole duration of the test. For this purpose, the prism was divided in four separate zones from the top to the bottom, as displayed in Figure 3.2. This spatial damage assessment tool is referred as the ***damage profiling approach***. For both spatial damage assessment tools mentioned above, a 95% confidence level margin of error was calculated according to Equation (1) for each "local" DRI numbers, which represents only the uncertainty related to the operator's repeatability. The DRI numbers were then compared according to the statistical/probabilistic methodology suggested by Ramsey and Schafer [21] (Figure 3.3).

Figure 3.1 : ***Grouped lines approach*** - Separation of the polished concrete section in groups of two lines for the comparison between the damage degree from the sides towards the core of the test prism.

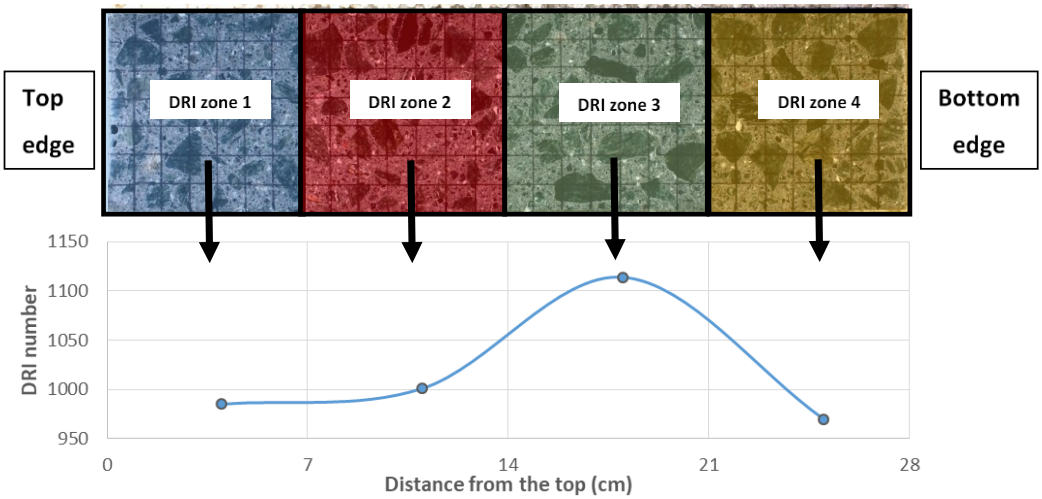

Figure 3.2 : ***Damage profiling approach*** - Separation of the polished concrete section in four zones for the determination of damage profile from the top (left) to the bottom (right) of the prism.

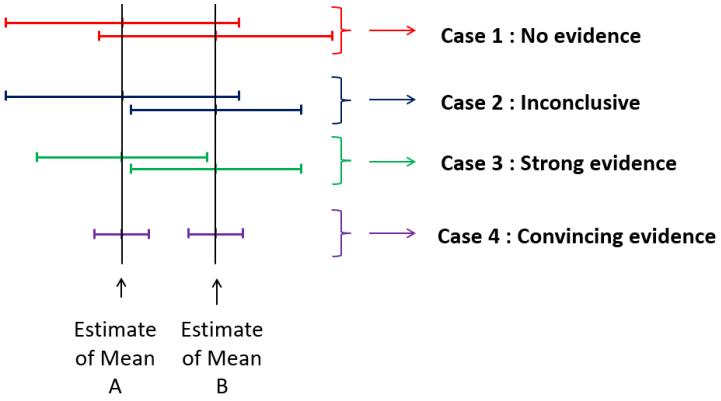

Figure 3.3 : Statistical/probabilistic methodology to draw conclusions when comparing DRI values and their respective margin of error based on a statistical approach. [21]

4. RESULTS

4.1 General

This section presents the results obtained with the *grouped lines approach* and the *damage profiling approach* for all analysed prisms. Considering the large number of assessed prisms (30), only typical examples are given while a summary of the results is provided in tables. The prisms were grouped in the five classes shown in Table 4.1 to ease comparison. Each class will have its own color in the summary tables. The legend used to compare DRI numbers in the summary tables is given in Table 4.1, while the statistical methodology applied is defined in Figure 3.3 (with a 95% confidence level).

Table 4.1: Legend of the summary tables provided in section 4.

√: there is a convincing evidence that a difference exists between the compared areas (95% confidence level)	(x): there is a strong evidence that a difference exists between the compared areas (95% confidence level)
(+): the difference between the two zones is positive i.e. Zone A > Zone B	**(-)**: the difference between the two zones is negative i.e. Zone A < Zone B
	Unwrapped prisms without SCMs and exposed to 38 or 60 °C
	Unwrapped prisms incorporating fly ash and exposed to 38 or 60 °C
	Unwrapped prisms incorporating slag and exposed to 38 or 60 °C
	Alkali wrapped prisms incorporating SCMs and exposed to 38 or 60 °C
	Alkali wrapped prisms without SCMs and exposed to 38 or 60 °C

4.2 Investigation of grouped lines

An overview of the grouped lines comparison between the external layer and the core of all the specimens analysed in this study is provided in Table 4.2. Figure 4.1a shows an example of the higher extent of damage in the external layer (L1) than the core (L2 & L3) of an alkali-wrapped prism with high expansion. A convincing or strong evidence of this feature was noticed on most (9/12) of the alkali-wrapped prisms, even some with low expansion like the 10U-4.12 specimen (Figure 4.1b). This convincing or strong evidence of damage difference was also noted on most (8/10) of the unwrapped prisms incorporating SCMs (either slag or fly ash) and exposed to 38 or 60°C, like shown in Figure 4.1c for the 17U-4.2 specimen. In the case of the unwrapped prisms without SCMs (controls) exposed to 38 or 60°C, a relatively similar damage degree was generally found between the external layer and the core, for expansion values equal or higher than 0.10%. On the other hand, no trend could be found for the only two unwrapped controls with expansion values lower than 0.10%. Examples for a low-expansion (2U-4.2) and a high-expansion unwrapped (control) specimen (3U-ASTM) are provided in Figure 4.1d and Figure 4.1e, respectively.

4.3 Damage profile

A typical example of the damage profile determined from a high-expansion prism is shown in Figure 4.2a (6U-4.2 specimen). A convincing evidence of lower damage degree within the top edge compared to the middle part of the that prism was observed. This feature was noted for most (9/12) prisms of expansion higher or equal to 0.10%, as shown in Table 4.3. However, none of the prisms with lower expansion showed a statistical evidence of a lower damage degree within their top edge. A typical example of damage profile obtained from a low-expansion (< 0.10%) specimen is provided in Figure 4.2b, where a somewhat uniform damage distribution was observed. Furthermore, according to Table 4.3, some (5/18) low-expansion specimens actually showed a strong or convincing evidence of higher damage degree in their bottom edge compared to their middle part. This tendency was less consistent for high-expansion specimens (≥ 0.10%). In fact, a strong or convincing evidence of lower damage degree within the bottom edge was observed for only 4 out of 12 high-expansion specimens, while a strong or convincing evidence of higher damage degree was reported in the bottom edge of only 2 out of 12 high-expansion specimens.

Table 4.2: Comparison of the extent of damage between the external layer (Line 1) and the core (Lines 2 and 3) of all assessed prisms using the *grouped lines approach*.

Specimen (Table 3.2)	Expansion (%)	Difference between L1 and L2	Difference between L1 and L3
1U-4.12	0.022	(x) **(+)**	
7U-ASTM	0.025	(x) **(+)**	(x) **(+)**
2U-4.2	0.026		(x) **(+)**
7U-4.2	0.026		
14U-4.12	0.028	(x) **(+)**	√ **(+)**
4U-4.2	0.032	(x) **(-)**	
10U-4.12	0.035	√ **(+)**	√ **(+)**
17U-3.12	0.038		
13U-4.2	0.039	√ **(+)**	√ **(+)**
14U-4.2	0.039	√ **(+)**	√ **(+)**
14U-ASTM	0.041	(x) **(+)**	
2U-4.12	0.041	(x) **(+)**	√ **(+)**
8U-4.2	0.053		(x) **(+)**
17U-4.2	0.055	√ **(+)**	√ **(+)**
13U-ASTM	0.055		
8U-ASTM	0.055	√ **(+)**	(x) **(+)**
10U-3.12	0.075	(x) **(+)**	(x) **(+)**
21U-ASTM	0.088	√ **(+)**	(x) **(+)**
11U-ASTM	0.100		(x) **(+)**
11U-3.12	0.113	(x) **(+)**	(x) **(+)**
4U-4.12	0.180		
3U-ASTM	0.216		
2U-3.12	0.221	(x) **(+)**	√ **(+)**
6U-4.2	0.230		
1U-3.12	0.234	√ **(+)**	√ **(+)**
15U-3.12	0.236		
15U-ASTM	0.240		
3U-3.12	0.244	√ **(+)**	√ **(+)**
6U-ASTM	0.254		√ **(-)**
11U-4.2	0.314		

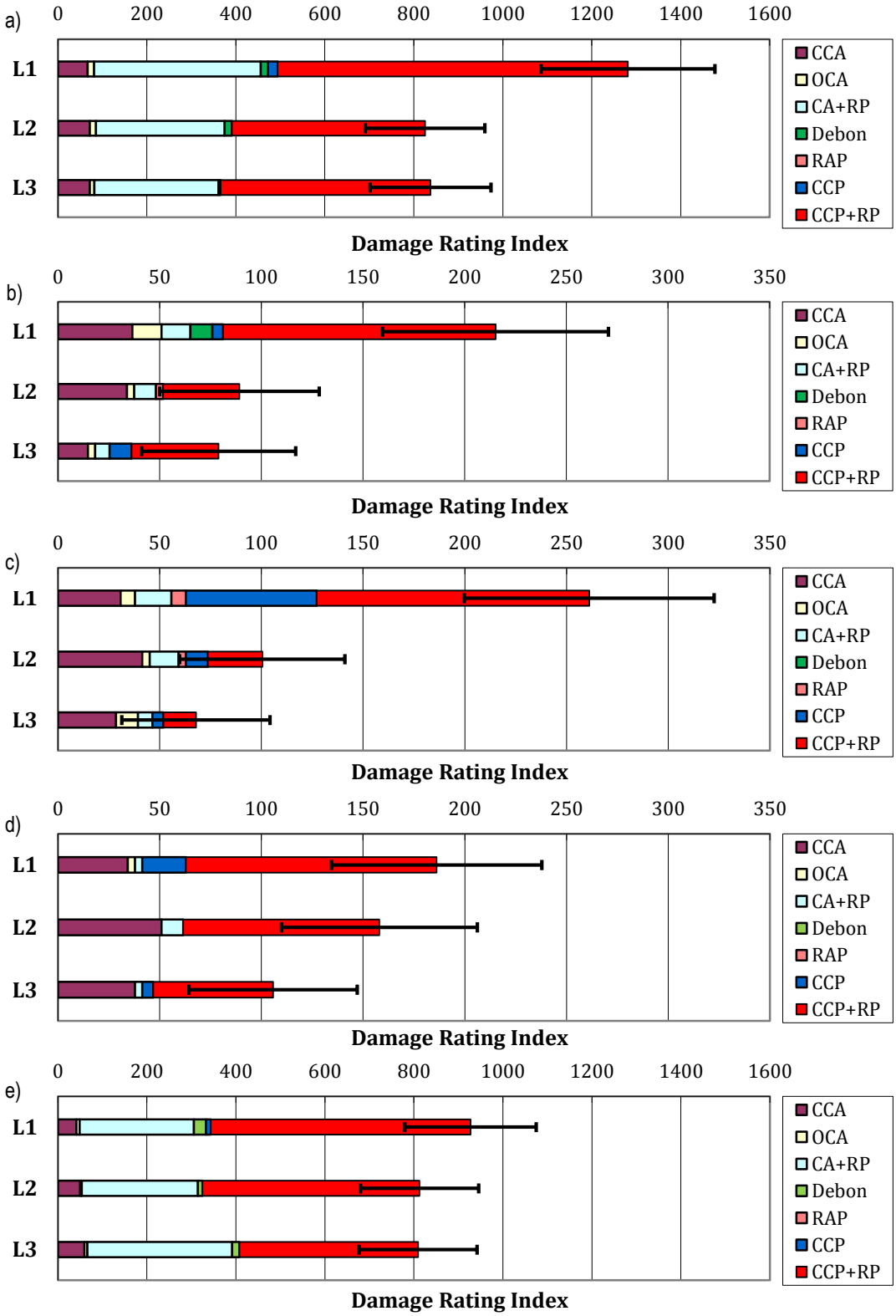

Figure 4.1 : Spatial distribution of damage (the acronyms are defined in Table 3.3) from the external layer (L1) to the core (L2 & L3) of a) the 1U-3.12 specimen, b) the 10U-4.12 specimen, c) the 17U-4.2 specimen, d) the 2U-4.2 specimen and e) the 3U-ASTM specimen. The margin of error was calculated using Equation (1).

Table 4.3: Comparison of the extent of damage between the edges (Zones 1 and 4) and the middle part (Zones 2 and 3) of the assessed prisms using the *damage profile approach*. The zones are defined in Figure 3.2.

Specimen (Table 3.2)	Expansion (%)	Difference between Zone 1 and Zone 2	Difference between Zone 1 and Zone 3	Difference between Zone 4 and Zone 2	Difference between Zone 4 and Zone 3
1U-4.12	0.022				
7U-ASTM	0.025				
2U-4.2	0.026			(x) **(-)**	
7U-4.2	0.026				
14U-4.12	0.028			√ **(+)**	(x) **(+)**
4U-4.2	0.032			(x) **(+)**	(x) **(+)**
10U-4.12	0.035	(x) **(+)**			
17U-3.12	0.038		(x) **(+)**	(x) **(-)**	
13U-4.2	0.039				
14U-4.2	0.039				
14U-ASTM	0.041				
2U-4.12	0.041			(x) **(+)**	(x) **(+)**
8U-4.2	0.053			√ **(+)**	(x) **(+)**
17U-4.2	0.055		√ **(-)**		
13U-ASTM	0.055			(x) **(-)**	
8U-ASTM	0.055			(x) **(+)**	
10U-3.12	0.075	(x) **(-)**	(x) **(-)**		
21U-ASTM	0.088	(x) **(-)**	(x) **(-)**		
11U-ASTM	0.100	(x) **(+)**		(x) **(+)**	
11U-3.12	0.113	(x) **(-)**	√ **(-)**		
4U-4.12	0.180	√ **(-)**	√ **(-)**	√ **(-)**	
3U-ASTM	0.216	(x) **(-)**		(x) **(-)**	(x) **(-)**
2U-3.12	0.221	(x) **(-)**	√ **(-)**	(x) **(+)**	
6U-4.2	0.230	√ **(-)**	√ **(-)**	(x) **(+)**	
1U-3.12	0.234	√ **(-)**	√ **(-)**		
15U-3.12	0.236			(x) **(-)**	(x) **(-)**
15U-ASTM	0.240		(x) **(-)**		
3U-3.12	0.244	(x) **(-)**	√ **(-)**		(x) **(-)**
6U-ASTM	0.254				
11U-4.2	0.314	√ **(-)**	√ **(-)**		

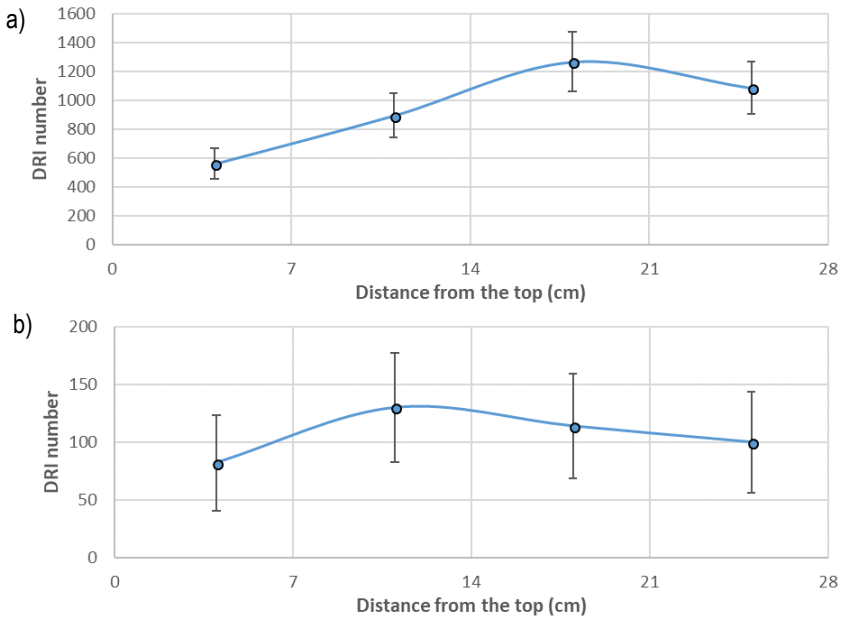

Figure 4.2 : Damage profile from the top to the bottom edges of a) the 6U-4.2 specimen and b) the 7U-4.2 specimen. The margin of error was calculated using the Equation (1).

5. DISCUSSION

5.1 General

The assessed prisms were selected based on the assumption that a damage gradient would be present within the specimens for different reasons. The first expected factor was moisture gradient, especially when SCMs were used in the mix. The second was alkali wrapping and its impact on damage close to the prism's surface. Finally, the leaching of alkalis was expected to play a major role on damage variations within the specimens. First, this section presents the main findings on how DRI was successfully able to detect damage variations within the same prism by addressing each tool separately. Then, a brief summary of the main findings about the impact of the laboratory testing conditions or the mix design on damage variations within the concrete prism is provided.

5.2 Reliability of the spatial damage assessment tools

5.2.1 External layer versus core of the prism

Investigating different sets of grouped lines provided a reliable overview on how the extent of damage spatially differs from the external layer to the core of the concrete specimens, especially because the margin of error allows to see if the DRI numbers are significantly different with respect to the uncertainty related to the operator performing the test. For instance, it was found that 80% of the unwrapped prisms incorporating SCMs (i.e. slag or fly ash) and exposed to 38 or 60°C display a convincing or strong evidence of a higher extent of damage within their external layer than their core (Table 4.2). It is assumed that the relatively lower permeability of the SCM binders might be responsible for this tendency. This is further discussed in section 5.3. Moreover, a convincing or strong evidence of a positive damage difference between the external layer and the core of the specimens was noticed for most (6/8) of the alkali wrapped prisms without SCMs, as shown in Table 4.2 (L1 vs L3). Accordingly, it is believed that providing a source of available/external alkalis can locally increase the rate and extent of damage induced by ASR. Furthermore, the results suggest that this effect is actually enhanced for concretes with lower alkali content, as further discussed in section 5.3. Another finding is the fact that most (6/8) of the control (i.e. no SCMs) unwrapped prisms showed a statistical evidence of equal or higher damage in their external layer than in their core. This is inconsistent with the numerical model developed by Multon and Sellier [35] for the advancement of ASR through a 70 mm cross-section prism (Figure 5.1).

It is possible that the core of the prism does not gain as much water as the external layer throughout the test. Therefore, a local race may exist between the reduction of alkalis due to leaching and the increase of reaction/damage enhanced by water ingress. This is also further discussed in section 5.3.

5.2.2 Damage profile from the top to the bottom edge of the prism

A significantly lower damage degree was found within the top edge of most of the specimens of expansion higher than 0.10% compared to their respective middle part, as displayed in Table 4.3. Since the prisms were always oriented the same way throughout the concrete prism test, alkali leaching resulting from the fall of condensed water from the top of the container to the top edge of the prism is assumed to be responsible for this finding. Interestingly, this lower damage degree at the top edge was noticed similarly for alkali wrapped and unwrapped specimens. This leads to the conclusion that the alkali wrapping method does not prevent leaching at the top edge of the prism even when stored in a sealed bag. The addition of water at the top edge of the test prism after each measurement could potentially be responsible for this alkali leaching/dilution at the top edge of the alkali wrapped specimens. Only a few statistically significant damage variation was observed on specimens with expansion lower than 0.10%, regardless of exposure conditions or mix design. However, the observed damage distribution within the latter was inconsistent. In approximately half of those specimens, the damage degree was lower within the edges compared to the middle part, whereas the opposite gradient was observed in the remaining specimens. This rather low capability to observe consistent damage variations in specimens with expansion lower than 0.1% can either be caused by the lack of repeatability of the method at such low damage degree (Equation (1)) or the rather negligible influence of leaching on the induced damage gradient at such low expansion.

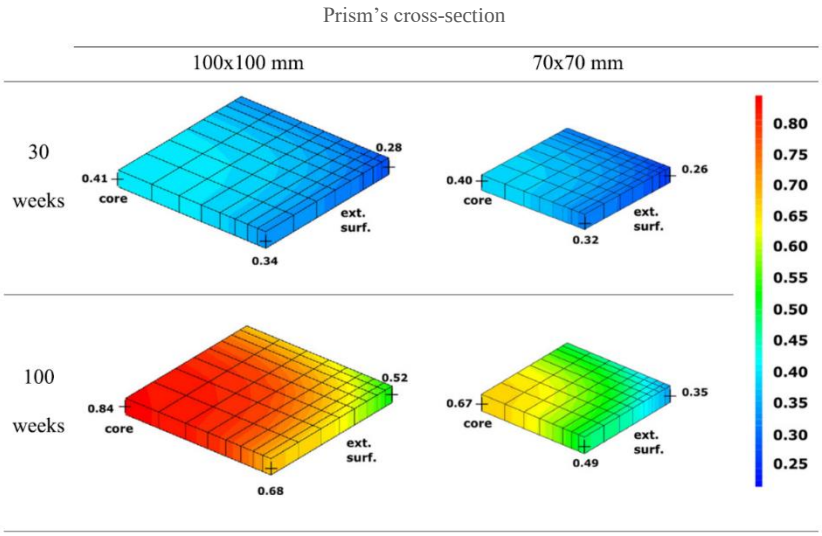

Figure 5.1 : Estimated advancement of ASR modelled using a multi-scale approach (aggregate and concrete scale) in the concrete prisms of Lindgård et al.'s [24] experiments after 30 and 100 weeks of CPT exposure. The scale is a relative percentage of the theoretical advancement of ASR in absence of alkali leaching (obtained by modeling) [35].

5.3 Main findings about the impact of mix design and exposure conditions on performance testing for ASR

This study aimed at evaluating whether statistically significant differences in damage could be detected within laboratory prisms exposed to different exposure conditions (temperature, alkali wrapping, etc.) and made with different binder types/contents (alkali content, SCMs, etc.). In order to do so, two damage profiling approaches were developed from the analysis of data generated through DRI determination. One must remember that the detected local damage variations within the specimens based on Equation (1) were purely assigned to the uncertainty related to the repeatability of the operator, which did not account for the "real" *measurement uncertainty* per say. Indeed, the latter requires the measurement to be repeated many times on independent specimens from the same set to limit the extent of so-called

sampling errors [36] and hence potentially "biased" conclusions. Despite the above limitation, some strong trends were observed by considering the sample as a whole.

The results obtained in this study suggest that despite being stored at high relative humidity, the prism's water content may not increase as fast as one might expect in their (inner) core during the test, even for a traditional and relatively small-size prism with a 0.45 w/b ratio, thus causing a gradient of water content in the test prism. As a result, a moisture gradient is likely created between the core and the external layer, resulting in higher early expansion and damage (cracking) generation in the outside layer of the test prisms, as witnessed by the grouped lines approach following DRI determination. This differential expansion/damage generation would then be maintained long enough until alkali leaching eventually stops the reaction. In a future experiment, analysing the moisture profile and the damage generation in companion prisms after different exposure time would allow to confirm whether a moisture gradient effectively affect the lateral damage profile in the prism throughout the test.

An even more pronounced gradient of water content in the test prism is likely to develop when a low permeability binder is used (Table 4.2). These binders would indeed allow less water absorption by the concrete resulting in a moisture gradient between the core and the external layer as reported by Lindgård et al. [25]. The latter could in turn induce a damage gradient like the one witnessed by DRI determination for SCM-bearing specimens.

Actually, even for control prisms (i.e. unwrapped and without SCMs), alkali leaching effects appear to reduce damage in the edges (i.e. top and bottom) and not in the external layer of the specimens. As suggested above, a local race may exist between the reduction of alkalis due to leaching and the increase of damage enhanced by water ingress. Therefore, it is suggested that more water gets in contact with the edges of the prism during the test than the external (vertical) layer, causing enhanced alkali leaching and thereby ASR reduction at the edges of the prism.

Providing an external source of alkalis through the alkali wrapping procedure implemented by Lindgård et al. [22, 24, 25] actually increases the extent of damage within the external layer of the prism compared to its core. It is expected to be caused by an increase in the rate and extent of ASR at the prism's surface in contact with the source of alkalis. Interestingly, the alkali content of the mix seems to influence this outcome, as shown in Table 5.1. In fact, most of the specimens (5/6) that show a statistical evidence of a damage gradient between the external layer and the core correspond to mixtures with a relatively low alkali content (i.e. clinker and added NaOH < 4.0 kg/m^3, Na_2O eq); on the other hand, half (1/2) of the specimens that did not show a statistical evidence of a damage gradient between the external layer and the core correspond to mixtures with a relatively higher alkali content from the clinker (i.e. clinker and added NaOH > 4.0 kg/m^3, Na_2O eq). Therefore, the results suggest that this effect is enhanced when the alkali content of the prism is somewhat low enough, i.e. less than ± 4.0 kg/m^3, Na_2O eq. Furthermore, the high level of damage measured in the internal layers of the low alkali specimen 1U-3.12 (DRI number ≈ 800; Figure 4.1) strongly suggests that alkalis can actually diffuse from the external layer to the core of the prism, because otherwise ASR would unlikely have occurred at such low alkali content (i.e. 1.5 kg/m^3, Na_2O eq). One can expect that ASR occurred earlier in the external layer thus causing the local damage difference noticed in this case.

Table 5.1 : Summary of the results when comparing the extent of damage within the core and the external layer of only the alkali wrapped specimens (either with or without SCMs). The legend is detailed in Table 4.1.

Specimen (Table 3.2)	Expansion (%)	Convincing or strong evidence of a difference between external layer and core of the prism (Table 4.2)	Alkali content (kg/m^3, Na_2O eq)
1U-4.12	0.022	(x) **(+)**	**1.5**
2U-4.12	0.041	√ **(+)**	2.0
11U-3.12	0.113	(x) **(+)**	**5.5**
4U-4.12	0.180		**2.0**
2U-3.12	0.221	√ **(+)**	2.0
1U-3.12	0.234	√ **(+)**	1.5
15U-3.12	0.236		**5.5**
3U-3.12	0.244	√ **(+)**	2.9

6. CONCLUSION

A new way to apply the results of DRI determination, i.e. as a spatial damage assessment tool, was investigated in this study. Two DRI spatial damage assessment tools were developed, i.e. the analysis of grouped lines and the damage profile. The former consists in separating the specimen in grouped lines of equal distance (laterally) from the prism's surface and the latter consists in separating the prism in four zones of equal area from the top to the bottom. A margin of error related to the operator's repeatability (Equation (1)) was used to compare the DRI numbers within the same specimen. The above tools were applied to a selected series of 30 concrete prisms tested for ASR performance testing through the concrete prism test (CPT). The assessed prisms were manufactured with different aggregates and binders as well as being exposed to different laboratory testing conditions, which were expected to induce internal damage variations/patterns. The main conclusions of this study are as follows:

- Both spatial damage assessment tools allowed to reliably detect damage variations within the assessed concrete prisms. This indicates that the DRI method is "sensitive" enough for damage spatial damage assessment if local damage variations are present within an area large enough, i.e. ± 50 cm^2. If the investigated area is smaller, the method's repeatability (i.e. same operator precision) may not be high enough to provide a relatively good indication of the extent of damage variations at such small scale. According to Equation (1), the "sensitivity" increases as a function of the size of the compared areas and the damage difference between them.
- The damage variations within prisms incorporating supplementary cementitious materials (SCMs) suggest that water ingress into the prism is significantly reduced due to lower permeability. This caused ASR-induced damage to be mainly located in the external layer of the prism, i.e. ± 1 cm from the surface.
- Providing an external source of alkalis through alkali wrapping increases the extent of damage within the external layer of the prism compared to its core. The results suggest that this effect is enhanced when the alkali content of the prism is low enough, i.e. less than ± 4.0 kg/m^3, Na_2O eq. Data also showed that alkalis from wrapping actually diffuse into the core of the test prism, thus resulting in higher internal damage even in concrete prisms with a very low original alkali content (that would not have induced ASR otherwise).
- The results suggest that damage reduction caused by alkali leaching are almost entirely concentrated at the top edge of the prisms (when prisms are always oriented the same way in the storage containers), and few evidence of significant damage reduction likely due to leaching was noticed at the external layer (sides) of the unwrapped control prisms. It is assumed that a local race may exist between the reduction of alkalis due to leaching and the increase of damage enhanced by the necessary water ingress. Therefore, ASR was enhanced by the presence of water at the beginning of the test in the external layer compared to the core of the prism, until alkali leaching stopped the reaction.

7. REFERENCES

1. Sanchez LFM, Fournier B, Jolin M, et al (2017) Overall assessment of Alkali-Aggregate Reaction (AAR) in concretes presenting different strengths and incorporating a wide range of reactive aggregate types and natures. Cement and Concrete Research 93:17–31. https://doi.org/10.1016/j.cemconres.2016.12.001

2. Gautam BP, Panesar DK (2017) The effect of elevated conditioning temperature on the ASR expansion, cracking and properties of reactive Spratt aggregate concrete. Construction and Building Materials 140:310–320. https://doi.org/10.1016/j.conbuildmat.2017.02.104

3. Rodrigue A, Duchesne J, Fournier B, et al (2020) Alkali-silica reaction in alkali-activated combined slag and fly ash concretes: The tempering effect of fly ash on expansion and cracking. Construction and Building Materials 251:118968. https://doi.org/10.1016/j.conbuildmat.2020.118968

4. Fecteau P-L, Fournier B, Duchesne J (2016) Use of SCMs on ACR-affected concrete: Expansion and damage evaluation through the Damage Rating Index. In: Proceedings of the 15th International Conference on Alkali-Aggregate Reaction (ICAAR). São Paulo (Brazil), p 10

5. Deschenes R, Giannini ER, Drimalas T, et al (2018) Mitigating Alkali-Silica Reaction and Freezing and Thawing in Concrete Pavement by Silane Treatment. ACI Materials Journal 115:. https://doi.org/10.14359/51702345

6. Allard A, Bilodeau S, Pissot F, et al (2016) Performance evaluation of thick concrete slabs affected by alkali-silica reaction (ASR) : Part I : material aspects. In: Proceedings of the 15th International Conference on Alkali-Aggregate Reaction (ICAAR). São Paulo (Brazil), p 10

7. Dehghan A, Zhang P, Ossetchkina E, et al (2019) Digital Microscopy Applied to Damage Rating Index for Alkali-Silica Reaction in Concrete. In: Cong D, Broton D (eds) Advances in Cement Analysis and Concrete Petrography. ASTM International, 100 Barr Harbor Drive, PO Box C700, West Conshohocken, PA 19428-2959, pp 105–125

8. Martin R-P, Sanchez L, Fournier B, Toutlemonde F (2017) Evaluation of different techniques for the diagnosis & prognosis of Internal Swelling Reaction (ISR) mechanisms in concrete. Construction and Building Materials 156:956–964. https://doi.org/10.1016/j.conbuildmat.2017.09.047

9. Champagne M, Roy-Tremblay M, Fournier B, et al (2019) Long-term effectiveness of sealers in counteracting alkali–silica reaction in highway median barriers exposed to wetting and drying, freezing and thawing, and de-icing salts. In: 17th Euroseminar on Microscopy Applied to Building Materials. Toronto (Canada), pp 155–162

10. Rivard P, Ballivy G, Gravel C, Saint-Pierre F (2010) Monitoring of an hydraulic structure affected by ASR: A case study. Cement and Concrete Research 40:676–680. https://doi.org/10.1016/j.cemconres.2009.09.010

11. Shrimer FH (2000) Application and use of Damage Rating Index in assessment of AAR-affected concrete - Selected case studies. In: Proceedings of the 11th International Conference on Alkali-Aggregate Reaction (ICAAR). Québec City (Canada). Québec City (Canada), pp 899–907

12. Hagelia P (2004) Origin of map cracking in view of the distribution of air voids, strength and ASR-gel. In: Proceedings of the 12th International Conference on Alkali-Aggregate Reaction (ICAAR). Beijing, China, p 12

13. Tavares Cavalcanti AJC, Alves Silveira JF (2000) AAR management at Paulo Afonso IV power plant - Brazil. In: Proceedings of the 11th International Conference on Alkali-Aggregate Reaction (ICAAR). Québec City (Canada), pp 1263–1272

14. MacDonald CA, Piersanti M, Shehata M, Magnan J (2019) Use of the Damage Rating Index (DRI) to evaluate level of deterioration due to alkali-silica reaction in 34-year old concrete from the Sudbury area. Toronto, Canada, pp 170–178

15. Rothstein D, Carrasquillo RL, Garza C (2012) Field and laboratory assessment of cracking damage from alkali-aggregate reactions in concrete slabs on ground, column footings and perimeter foundations, midwest USA. In: Proceedings of the 14th International Conference on Alkali-Aggregate Reaction (ICAAR). Austin (Texas), p 10

16. Lindgård J, Hammer TA, Skjølsvold O, et al (2017) 236661 KPN-ASR - Test report 1. SINTEF Building and Infrastructure, Trondheim (Norway)

17. Clemeña GG, Lane DS, Freeman TE, Lozev MG (2000) Evaluation of nondestructive evaluation methods for application in early detection of deterioration in concrete pavements. Virginia Transportation Research Council, Charlottesville, Virginia, USA

18. Grattan-Bellew PE, Danay A (1992) Comparison of laboratory and field evaluation of alkali-silica reaction in large dams. In: Marc-André Bérubé Symposium on Alkali-Aggregate Reaction (AAR) in Concrete, Montréal (Canada), May 2006, B. Fournier Editor, CANMET-MTL, 21-44. Fredericton (Canada), pp 1–23

19. Sanchez LFM, Fournier B, Jolin M, Duchesne J (2015) Reliable quantification of AAR damage through assessment of the Damage Rating Index (DRI). Cement and Concrete Research 67:74–92. http://dx.doi.org/10.1016/j.cemconres.2014.08.002

20. Champagne M (2020) Applying the Damage Rating Index for the spatial damage assessment in concrete specimens affected by alkali-silica reaction (ASR). MSc Thesis, Université Laval

21. Ramsey F, Schafer D (2002) The Statistical Sleuth A Course in Methods of Data Analysis, 2nd Edition. Cengage Learning, Boston, MA 03310

22. Lindgård J, Rønning TF, Thomas MDA, et al (2016) ASR - performance testing: Main findings in the Norwegian COIN project. In: Proceedings of the 15th International Conference on Alkali-Aggregate Reaction (ICAAR). São Paulo (Brazil)

23. Wigum BJ, Lindgård J (2016) RILEM technical committees (TCS) - Past and present. TC 258-AAA: Avoiding alkali aggregate reaction (AAR) in concrete - Performance based concept (2014 - 2019). In: Proceedings of the 15th International Conference on Alkali-Aggregate Reaction (ICAAR). São Paulo (Brazil)

24. Lindgård J, Thomas MDA, Sellevold EJ, et al (2013) Alkali–silica reaction (ASR)—performance testing: Influence of specimen pre-treatment, exposure conditions and prism size on alkali leaching and prism expansion. Cement and Concrete Research 53:68–90. https://doi.org/10.1016/j.cemconres.2013.05.017

25. Lindgård J, Sellevold EJ, Thomas MDA, et al (2013) Alkali–silica reaction (ASR)—performance testing: Influence of specimen pre-treatment, exposure conditions and prism size on concrete porosity, moisture state and transport properties. Cement and Concrete Research 53:145–167. https://doi.org/10.1016/j.cemconres.2013.05.020

26. CSA A23.2-14A (2019) Potential expansivity of aggregates (procedure for length change due to alkali-aggregate reaction in concrete prisms at 38 °C). In: Concrete materials and methods of concrete construction/Test methods and standard practices for concrete. CSA Group. Mississauga (Canada). pp 495–508

27. Norwegian Concrete Association (2005) Alkali–aggregate reactions in concrete, Test methods and Requirements to Test Laboratories. Publ. no. 32 (NB32), Oslo, Norway

28. Lindgård J, Nixon PJ, Borchers I, et al (2010) The EU “PARTNER” Project — European standard tests to prevent alkali reactions in aggregates: Final results and recommendations. Cement and Concrete Research 40:611–635. https://doi.org/10.1016/j.cemconres.2009.09.004

29. Villeneuve V, Fournier B, Duchesne J (2012) Determination of the damage in concrete affected by ASR - The Damage Rating Index (DRI). In: Proceedings of the 14th International Conference on Alkali-Aggregate Reaction (ICAAR). Austin (Texas). Austin (Texas), p 10

30. Sanchez LFM, Fournier B, Jolin M, et al (2017) Overall assessment of Alkali-Aggregate Reaction (AAR) in concretes presenting different strengths and incorporating a wide range of reactive aggregate types and natures. Cement and Concrete Research 93:17–31. https://doi.org/10.1016/j.cemconres.2016.12.001

31. Sanchez L, Fournier B, Jolin M, et al (2016) Use of Damage Rating Index to Quantify Alkali-Silica Reaction Damage in Concrete: Fine versus Coarse Aggregate. ACI Materials Journal 113:395–407. https://doi.org/10.14359/51688983

32. RILEM TC 106-AAR: Alkali-Aggregate Reaction (2000) B-TC 106-3-Detection of potential alkali-reactivity of aggregates-Method for aggregate combinations using concrete prisms. Mat Struct 33:290–293. https://doi.org/10.1007/BF02479698

33. RILEM Recommended Test Method: AAR-4.1 (2016) Detection of Potential Alkali-Reactivity—60 °C Test Method for Aggregate Combinations Using Concrete Prisms. In: RILEM Recommendations for the Prevention of Damage by Alkali-Aggregate Reactions in New Concrete Structures. Springer Netherlands, Dordrecht, pp 99–116

34. ASTM C1293 (2015) Test Method for Determination of Length Change of Concrete Due to Alkali-Silica Reaction

35. Multon S, Sellier A (2016) Multi-scale analysis of alkali–silica reaction (ASR): Impact of alkali leaching on scale effects affecting expansion tests. Cement and Concrete Research 81:122–133. https://doi.org/10.1016/j.cemconres.2015.12.007

36. Särndal C-E, Swensson B, Wretman J (1992) Model Assisted Survey Sampling. Springer-Verlag, New York